applied sciences

MDPI

Article

An Optimal Sizing Design Approach of Hybrid Energy Sources for Various Electric Vehicles

Syuan-Yi Chen [1], Chu-Yang Chiu [2], Yi-Hsuan Hung [3,*], Kuo-Kuang Jen [4], Gwo-Huei You [4] and Po-Lin Shih [4]

[1] Department of Electrical Engineering, National Taiwan Normal University, Taipei 106, Taiwan; chensy@ntnu.edu.tw
[2] Department of Industry Education, National Taiwan Normal University, Taipei 106, Taiwan; 60970017h@ntnu.edu.tw
[3] Undergraduate Program of Vehicle and Energy Engineering, National Taiwan Normal University, Taipei 106, Taiwan
[4] National Chung-Shan Institute and Science & Technology, Taoyuan 325, Taiwan; rgg1201@gmail.com (K.-K.J.); tagifan@yahoo.com.tw (G.-H.Y.); r22263222@gmail.com (P.-L.S.)
* Correspondence: hungyh@ntnu.edu.tw

Featured Application: This method provided an effective design method for multiple electric energy sources for various electric vehicles such as: electric buses, electric forklifts, electric sports cars, etc. in order to optimize the cost, weight, traveling mileage, etc. under the preset constraints.

Abstract: In this paper, we present a discussion about green energy sources that have been widely utilized in electric vehicles (EVs). To achieve different requirements of various EVs, the correct sizing of energy sources is crucial so that the cost and output performance will be optimized. In this research, three energy sources, supercapacitors (SCs), lithium titanate oxide (LTO) batteries, and Nickel Manganese Cobalt (NCM) (or Li3) batteries, were considered for hybridization. An effective global search algorithm (GSA) was designed for optimal sizing of hybrid electric energy systems (HEESs). The GSA procedures were: (1) vehicle specification and performance requirements of energy sources, (2) determination of cost function and constraints, (3) GSA optimization with for-loops, (4) optimal results. Five examples of EVs, the electric sedan, long-distance electric bus, short-distance electric bus, electric forklift, and electric sports car, were analyzed for optimal hybrid energy combination under different criteria and specifications. The GSA effectively optimized the designs of energy sizing. The performance indices and vehicle requirements studied were the specific price, specific energy at a constant volume, specific energy at a constant mass, and specific power at a constant mass for three energy sources, SCs, LTO batteries, and Li batteries. The vehicle requirements including the maximum output power, vehicle acceleration, climbability, and maximum speed have been formulated as the design constraints. A numerical analysis of five types of EVs was analyzed for optimal sizing of the HEES and the optimal position of the DC/DC converter with the lowest cost function. The integrated system and control designs of the HESS using the GSA, more applications for green energy sources, and different types of EVs will be studied in the future.

Keywords: electric vehicle; optimal sizing; lithium titanate oxide (LTO); supercapacitor (SC); global search algorithm

check for updates

Citation: Chen, S.-Y.; Chiu, C.-Y.; Hung, Y.-H.; Jen, K.-K.; You, G.-H.; Shih, P.-L. An Optimal Sizing Design Approach of Hybrid Energy Sources for Various Electric Vehicles. *Appl. Sci.* **2022**, *12*, 2961. https://doi.org/10.3390/app12062961

Academic Editor: Daniel Villanueva Torres

Received: 20 November 2021
Accepted: 7 March 2022
Published: 14 March 2022

Publisher's Note: MDPI stays neutral with regard to jurisdictional claims in published maps and institutional affiliations.

Copyright: © 2022 by the authors. Licensee MDPI, Basel, Switzerland. This article is an open access article distributed under the terms and conditions of the Creative Commons Attribution (CC BY) license (https://creativecommons.org/licenses/by/4.0/).

1. Introduction

Due to the stringent transportation laws legislated, especially for fuel economy, electric vehicles (EVs) have attracted much more attention recently due to their characteristics of zero pollutants, low noise, high efficiency, and rapid acceleration compared to traditional engine vehicles [1]. The most popular EV type is the battery EV (BEV) with one type of battery, such as LiFePO4 batteries, lithium titanate oxide (LTO) batteries, nickel manganese cobalt (NMC) batteries, or nickel cobalt aluminium (NCA) batteries [2]. Each battery

type is characterized by specific energy, specific power, cell voltage, C-rate for charge and discharge, life cycle, inner resistance, cost, etc. [3]. Hence, choosing the correct type of battery according to the requirements and specifications of the target vehicle is crucial.

Recently, a hybridization concept for the powertrains or energy sources has been needed due to the physical constraints of a sole power source or single energy source that limit the performance of EVs. To solve this problem, the most popular hybrid powertrains are an engine/motor/generator hybrid system such as the full hybrid system (i.e., Toyota THS) and a power-assist hybrid system (i.e., Honda Insight). The electric power devices effectively compensate for the inefficient operation and high pollution at low-power or low-speed conditions, recover the braking energy from generation, and properly assist the traction torque in low-torque areas [4]. Hybrid electric energy sources such as the fuel cell (FC)/battery system [5], the battery/SC system [6], the fuel cell/SC system [7], and even the FC/battery/SC hybrid system [8] have been employed to EVs. The FC system provides the stable output power to the out load; meanwhile, it charges the energy storage devices (such as batteries and SCs) when the State-Of-Charges (SOCs) of the energy storage devices are low [9]. Contrarily, the SC system plays the role of providing the boost power while the vehicle accelerates with high power, or receiving the brake regeneration power with high efficiency due to low inner resistance [10]. The battery system is able to drive the vehicle at a wide-power-range operation while storing the extra or recovered energy from outside [11]. To extend the life cycle and maintain the state-of-health (SOH) of the battery, SCs compensate the peak power to avoid the high C-rate discharge or even high C-rate charge.

For hybrid electric energy systems (HEESs), two main approaches are utilized to enhance the system performance to increase the overall system efficiency. The first approach is the energy management control. Three categories are summarized for the control. The first is the rule-based control [12], where the flowchart decision making [13] (if-else control, fuzzy logic control [14], etc.) relies on engineering intuition. The second is the theoretical-based control, such as deterministic dynamics programming (DDP) or the Genetic Algorithm (GA), where the computational resource is extremely high [15]. It leads to the offline optimization [16]. The third is the online optimization, which combines the theories integrated into rules such as stochastic dynamics programming (SDP) [17] bionic optimization [18], the equivalent consumption minimization strategy [19,20], etc.

Though the energy management control improves the system performance, the second approach, system design, is more crucial, as the optimal sizing of an HEES directly influences the maximal output performance, total stored energy, and even the cost, occupied space, and the gross weight [21]. For HEES sizing, in [22], a hybrid battery system (HBS) with NCA and LTO batteries of an EV was evaluated to reduce battery aging and extend the life cycle. Four structures, mono battery, passive HBS, active HBS with one DC/DC converter, and active HBS with two DC/DC converters, were compared. In [23], a high energy storage and a high power storage were combined. The positions of the DC/DC converter influenced the total consumed energy in the beginning of life (BoL) and end of life (EoL). The main contributions of this research are summarized as: (1) the performance indices of three energy sources, SCs, LTO batteries, and NCM batteries (in abbreviation, Li3, later) were studied and compared; (2) the GSA for the HEES was developed with four steps; (3) the HEESs of five types of EVs (electric sedan, electric forklift, short-distance electric bus, long-distance electric bus, and electric sports car) were optimized for sizing. The optimal positions of the DC/DC converters were found as well. The experimental assessment will be conducted in the future.

2. Development of Global Search Algorithm for HEESs

2.1. The Configuration of HEESs

According to our literature review, the four configurations of HEESs are separated as shown in Figure 1. They are: (1) active, (2) passive, (3) active–passive type 1 and (4) active–passive type 2. For the active type (Figure 1a), two DC/DC converters are equipped

at the rear parts of dual energy sources, respectively. By properly controlling the control unit, the energy management is determined by two converters while the output voltages are stabilized at the downstream of the converters. The drawbacks of (1) are the extra cost and occupied volume of the converters. For passive type, the in/out energy flows of two energy sources are determined only by output voltages of the two sources without the energy management. Though the cost is lowest and the structure is simplest, the state-of-health (SOH) of both sources might decrease rapidly due to improperly drawn currents or lack of SOC control. For active–passive type 1, one DC/DC converter is at the output of the Li3 battery. As the output current (power) of the DC/DC converter is controlled while the output voltage is stabilized, the output power of the LTO is passively given. For active–passive type 2, one DC/DC is at the output of the LTO battery. As the output current (power) of the DC/DC is controlled while the output voltage is stabilized, the output power of the Li3 is passively given. Both active–passive types exhibit the same performance as that of the active type. However, the overall system efficiency is higher because the extra input/output power loss of the second converter is absent. Moreover, the system cost and occupied volume and weight are lower due to the single DC/DC converter. Though the cost is higher than that of the passive type, the SOH of dual energy sources can be extended to lower the cost. Of these four types, two active–passive types were chosen for system sizing optimization. The position of the single DC/DC converter was selected using the proposed GSA. Note that the system efficiency of hybrid energy sources is significantly higher than that of the single source, especially at the EoL period [23]. Hence, the single-source system was not considered in this research.

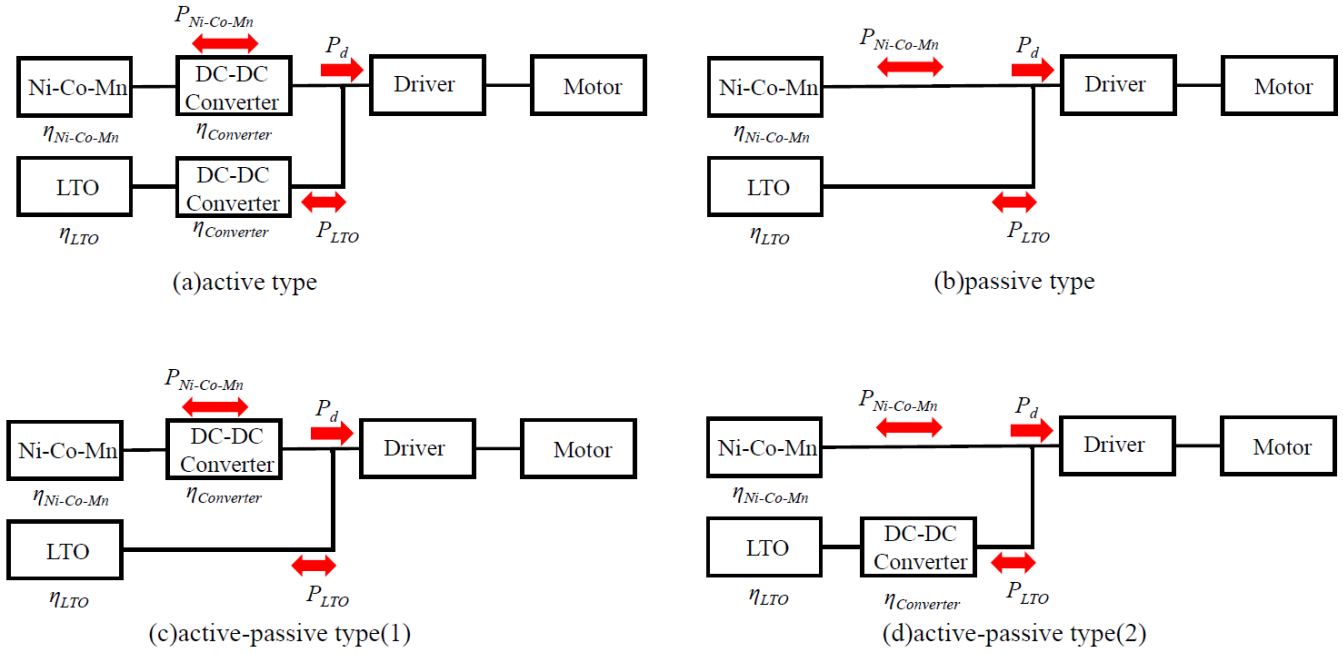


Figure 1. Configurations of the HEES.

2.2. The Procedures of the GSA

In this section, we developed the GSA for HEESs of EVs. The procedure was separated into four steps: (1) vehicle specification and performance requirements of energy sources, (2) determination of cost function and constraints, (3) GSA optimization with for-loops, (4) optimal results. The following is the procedure of the proposed GSA:

(1) Vehicle specification and performance requirements of energy sources; in this step, two phases are designed separately. The first phase is the performance indices of energy sources, while the second phase is the specification of requirements of the target vehicle. The performance indices of energy sources are: (a) specific energy (kWh/kg or kWh/L) (the energy stored in a constant mass or in a constant volume), as the higher the specific

energy, the more electric energy is able to be released to drive the traction motor in an EV so that the traveling mileage is larger; (b) specific power (kW/kg or kW/L) (the maximized power that can be released in a constant mass or in a constant volume), as the higher the specific power, the more electric power is able to propel the traction motor so that the values of vehicle acceleration and maximum vehicle speed are higher; and (c) specific price (USD/kWh) (the cost for energy capacity of 1 kW-hr), as the lower the specific cost, at a constant stored energy, the lower the overall cost [24].

The second phase is the vehicle requirements and specification. The key indices are (a) traveling mileage; (b) maximal power; (c) climbability; and (d) acceleration. These indices are criteria for target cost function, which will be described later. For traveling mileage, it is correlated to the energy stored in the HEES. For a chosen specific driving cycle, the consumed energy for one cycle as well as the traveling distance can be calculated by the following two equations:

$$E = \int_0^t P_t dt = \int_0^t (F(t) \times V(t)) dt \tag{1}$$

$$D \sum_{i=0}^{n} V(t) \times t_i \tag{2}$$

where E, P, F, D, V, and t represent energy demand, power demand, traction force of the wheel, distance, vehicle velocity, and time step, respectively; the subscript i represents the driving time(s). Hence, the total distance decides the minimum requirement of energy storage. For maximal power, it is related to the tested initial speed, target speed, and the varied vehicle mass determined by the HEES sizing. The two following equations are listed as [3,4]:

$$P_{max} \approx 2 \times \Delta E \times \Delta t^{-1} \tag{3}$$

$$\Delta E = \frac{M_{veh}}{2} \left({V_{init}}^2 - {V_{goal}}^2 \right) \tag{4}$$

where P_{max}, ΔE, Δt, and M represent maximum power demanded, kinetic energy, demanded time(s), and mass, respectively; the subscripts veh, $init.$, and $goal.$ represent vehicle, initial, and goal, respectively.

For climbability, it is correlated with the maximum power requirement as well. Modified from Equations (5)–(8), the calculated power is formulated as:

$$F_{climb} = M_{veh} g \cos\theta \tag{5}$$

$$F_{roll} = \mu M_{veh} g \sin\theta \tag{6}$$

$$F_{wind} = \frac{M_{veh} C_d \rho A_f V^2}{2} \tag{7}$$

$$M_{veh} \frac{dV}{dt} = \frac{\tau_w}{r_w} - F_{climb} - F_{roll} - F_{wind} \tag{8}$$

where F, g, θ, μ, C_d, ρ, A_f, r, and τ represent force, gravity acceleration, road slope, rolling coefficient, aero drag coefficient, air density, frontal area, radius, and traction torque, respectively; the subscripts $climb$, $roll$, $wind$, and w represent climbing resistance, rolling resistance, wind resistance, and wheel, respectively. For acceleration, it can be determined by the profiles in Figure 2.

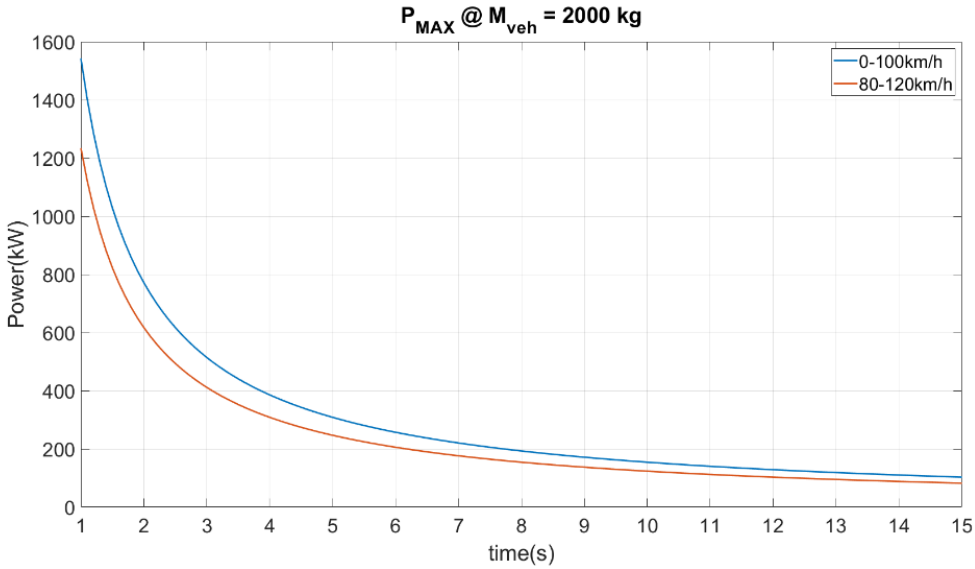


Figure 2. The power variations with different acceleration settings (example).

(2) Determination of the cost function and constraints; to optimize the HEES, the variable of the cost function is set to be the total cost of the HEES. It can be listed as:

$$C_{HEES} = C_{li3} + C_{LTO} \tag{9}$$

where C is cost, and the subscripts $HEES$, $li3$, and LTO represent the HESS, Li3 battery, and LTO battery set, respectively. Individual costs of dual energy sources are listed as:

$$C_{li3} = E_{HEES}(j) \times SR(k) \times SP_{li3} + \frac{E_{HEES}(j) \times SR(k) \times PD_{li3}}{SW_{li3}} \times [SPDC(\mathrm{X}(i))] \tag{10}$$

$$C_{LTO} = E_{HEES}(j) \times SR(k) \times SP_{lto} + \frac{E_{HEES}(j) \times SR(k) \times PD_{lto}}{SW_{lto}} \times [SPDC(1 - \mathrm{X}(i))] \tag{11}$$

where E, SR, SP, PD, SW, $SPDC$, i, j, and k represent stored energy, size ratio, specific price (USD/kWh), power density (kw/kg), specific weight (kWh/kg), specific price of DC/DC converter (USD/kW), index for searching the DC/DC converter, index for searching energy of HEES, and index for searching the size ratio, respectively.

Thus the cost function J can be defined as follows:

$$J(i,j,k) = C_{li3}(i,j,k) + C_{LTO}(i,j,k) + \gamma(i,j,k) \tag{12}$$

subject to

$$D_{li3} + D_{LTO} \geq D_{max} \tag{13}$$

$$P_{li3} + P_{LTO} \geq P_{max} \tag{14}$$

$$V_{li3} + V_{LTO} \leq V_{max} \tag{15}$$

$$W_{li3} + W_{LTO} \leq W_{max} \tag{16}$$

$$\gamma(i,j,k) = \begin{cases} 0 & \textit{if above equlation satisfied} \\ 10^6 & \textit{if above equlation unsatisfied} \end{cases} \tag{17}$$

where V, W, and γ represent volume, weight, and penalty value, respectively.

(3) GSA optimization with for-loops; after deriving the cost function, performance requirements, and the performance indices of dual energy sources, the GSA was proposed, as shown in Figure 3. First, three for-loops were constructed. The most outer loop was the DC/DC position with two possible values: $i = [0, 1]$. The second loop was the required total energy of the HESS with bounded values from $E_{HEES,min}$ to $E_{HEES,max}$. The increment of $E_{HEES,inc}$ separated for the index of E_{HEES} was from $j = 1$ ($E_{HEES,min}$) to $j = n$ ($E_{HEES,max}$). The total number n was calculated by: $n = \frac{[E_{HEES,max} - E_{HEES,min}]}{E_{HEES,inc}} + 1$. The most inner loop was the size ratio with bounded values from 0 to 1. The increment of SR_{inc} separated the index of SR from $k = 1$ ($SR = 0$) to $k = m$ ($SR = 1$). The total number m was calculated from: $m = \frac{[1-0]}{SR_{inc}} + 1$. Therefore, the possible combinations of DC/DC converter positions, total energies of the HEES, and size ratios were $2 \times n \times m$ cases. At each case with a determined DC/DC converter position, total HEES energy, and size ratio, the energy of the Li3 battery was $E_{li3} = E_{HEES}(j) \times SR(k)$, while the energy of the LTO battery was $E_{LTO} = E_{HEES}(j) \times [1 - SR(k)]$.

Next, physical constraints were calculated based on Equations (13)–(16) including D_{max}, P_{max}, V_{max}, and W_{max}. The value of γ can be determined if any of the constraints are satisfied or unsatisfied. The three-dimensional database with indices $i, j,$ and k was constructed.

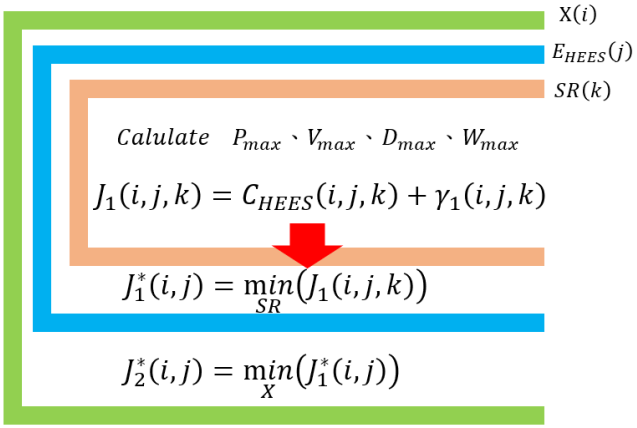


Figure 3. The nested for-loop structure for the GSA.

(4) Optimal results; to determine the optimal solution at a specific DC/DC converter position and stored hybrid energy, the cost functions with various size ratios were compared. The cost function with a minimum value under a chosen size ratio was the best solution, while the size ratio was the optimal size ratio at a specific X (position of DC/DC converter). That is:

$$J_1{}^*(i,j) = \min_{SR}(J_1(i,j,k)) \tag{18}$$

Next, for the outer layer, using different DC/DC converter positions, the final optimal solution can be determined and chosen from $J_1{}^*$.

$$J_2{}^*(j) = \min_{X}(J^*{}_1(i,j)) \tag{19}$$

Figure 4 summarizes the flow chart of the GSA for optimal size ratio: (1) vehicle specification and performance requirements of energy sources, (2) determination of the cost function and constraints, (3) GSA optimization with for-loops, and (4) optimal results. Using the four steps, the optimal HEES will be found.

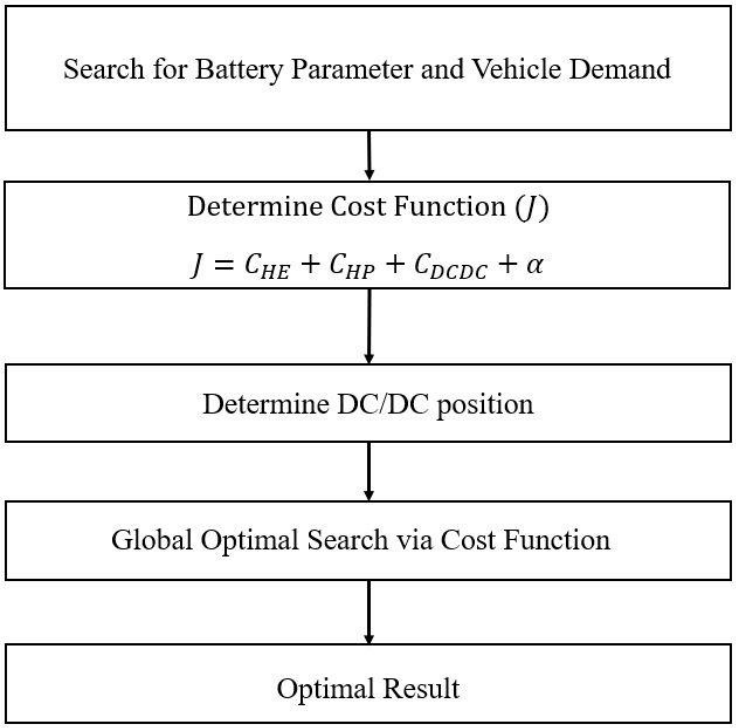


Figure 4. Flowchart of the GSA for HEESs.

3. Case Study for Five Types of Electric Vehicles

3.1. Electric Sedan

With the rapid popularization of commercialized electric sedans, all international automakers have produced several types of EVs. However, the trade-off between high power (good acceleration and high maximum speed) and high energy (traveling mileage) makes a vehicle with a single energy source difficult to produce. To optimize the HEES, the cost function is listed as follows:

$$J = E_{HEES} \times SR \times SP_{HP} + E_{HEES} \times (1 - SR) \times SP_{HE} + C_{DCDC} + \gamma \tag{20}$$

where the optimized cost is calculated by the summation of the cost of a high power source (LTO), the cost of a high energy source (Li3), and the cost of a DC/DC converter. The constraints are as follows:

$$\begin{aligned} P_{max} &\begin{cases} 0.95 \times (P_{HE} + P_{HP}) > P_{max} \\ P_{HE,max} = \frac{E_{HE}}{SW_{HP} \times SP_{HP}} \\ P_{HP,max} = \frac{E_{HEES} - E_{HE}}{SW_{HE} \times SP_{HE}} \end{cases}, \\ C_{max} &\begin{cases} C_{HE} + C_{HP} + C_{DCDC} < 1.22 \times C_{HP} \\ C_{HE} = E_{HEES} \times SR \times SP_{HE} \\ C_{HP} = E_{HEES} \times (1 - SR) \times SP_{HP} \\ C_{DCDC} = P_{HP} \times SPDC \times x(i) + P_{HE} \times SPDC \times [1 - x(i)] \end{cases} \\ W_{max} &\begin{cases} W_{HE} + W_{HP} < 1.22 \times W_{HE} \\ W_{HE} = \frac{E_{HE}}{SW_{HE}} \\ W_{HP} = \frac{E_{HEES} - E_{HE}}{SW_{HP}} \end{cases}, D_{max} \left\{ E_{HEES} > \frac{P_{50} \times D_{max} \times 3600}{1000 \times 50} \right. \end{aligned} \tag{21}$$

where the constants 0.95, 1.22, and P_{50} represent battery efficiency, safety factor, and power demand at the constant velocity of 50 km/h, respectively. Because the battery efficiency was influenced by SOC, which varies for energy management but not for the sizing optimization, the efficiency was set as a constant average value of 95%. For the safety factor, 1.22, for the weight, cost, and volume, the references [25,26] were considered. The subscripts *HE*

and *HP* represent a high-energy and high-power battery, respectively. To satisfy the first constraint, P_{max}, the maximal power of high energy or the high power were derived from the electric capacity divided by the specific weight and the specific price. The maximum cost of the HEES was a factor (1.22) multiplied by the summation of the total cost of the LTO batteries, Li3 batteries, and the DC/DC converter. The maximum weight of the HEES was an allowable factor (i.e., 1.22) multiplied by the summation of the total weight of the LTO batteries and the Li3 batteries. The minimum electric capacity was calculated by giving the required traveling distance at a constant speed of 50 km/h. With the boundary conditions of these four limitations, the optimal cost function concerning the vehicle performance requirement can be globally searched for.

3.2. Electric Forklift

Similar to Section 3.1, the cost function was the total cost of the HEES with a penalty factor. The major concern was the required maximum power while the forklift lifts up the goods. Hence, in Equation (22), the summation of the dual power sources multiplied by an efficiency factor (i.e., 0.95) needs to be higher than a preset maximum power value.

$$0.95 \times (P_{HP} + P_{HE}) > P_{max} \tag{22}$$

3.3. Long-Distance Electric Bus

For the long-distance electric bus, the traveling distance was crucial. As Equation (20) shows, the cost function was the total cost of the HEES to be minimized. The major concern was the required maximum power. The summation of the stored energy needed to be higher than a preset value for a long traveling distance. Due to the limited space of the chassis to mount the HEES system, the summation of the occupied volume of dual sources multiplied by a safety factor (1.22) needed to be smaller than a preset space (V_{max}).

$$\begin{array}{c} 0.95 \times (P_{HP} + P_{HE}) > P_{max} \\ E_{HP} + E_{HE} > E_{max} \\ 1.22(V_{HP} + V_{HE}) < V_{max} \end{array} \tag{23}$$

3.4. Short-Distance Electric Bus

For the short-distance electric bus, the traveling distance was a minor concern due to a fixed route for operation. Instead, the weight of the HEES, which influences the power consumption during frequent acceleration and deceleration, was crucial. Hence, the major concern was the HEES weight, which needed to be less than a preset value (W_{max}). Next, the summation of the HEES multiplied by an efficiency factor (i.e., 0.95) needed to be higher than a preset maximum power as well. Due to the limited chassis space to mount the HEES system, the summation of the occupied volume of dual sources multiplied by a safety factor (1.22) needed to be smaller than a preset space.

$$\begin{array}{c} 0.95 \times (P_{HP} + P_{HE}) > P_{max} \\ W_{HE} + W_{HP} < W_{max} \\ 1.22(V_{HP} + V_{HE}) < V_{max} \end{array} \tag{24}$$

3.5. Electric Sports Car

For the electric sports car, the HEES weight was a key issue because of the stringent requirement of acceleration and deceleration. Hence, the major concern was the HEES weight, which needed to be less than a preset value (W_{max}). Next, the maximum vehicle speed was correlated to the maximum output power, so the summation of the HEES multiplied by an efficiency factor (i.e., 0.95) needed to be higher than a preset value. The limited

space for the HEES was another concern, where the summation of the occupied volume of dual sources multiplied by a safety factor (1.22) must be smaller than a preset space.

$$\begin{gathered} 0.95 \times (P_{HP} + P_{HE}) > P_{max} \\ W_{max} < W_{HE} + W_{HP} \\ 1.22\ (V_{HE} + V_{HP}) < V_{max} \end{gathered} \tag{25}$$

From the constraints proposed for the five types of vehicles, the GSA is developed in Section 2 and will search for the optimal size ratio and the proper position of the DC/DC converter.

4. Simulation Results and Discussion

Firstly, the parameters and specifications of energy sources including the specific power, specific price, specific energy at constant volume, and specific energy at constant mass were searched and averaged for further use. Then, the performance with respect to size ratio for the cases of SC and Li3 battery and LTO and Li3 battery were simulated. Next, the sizing of five types of EVs was analyzed using the GSA.

4.1. Parameters and Specifications of Energy Sources

The performance indices of three energy storage devices (SC, LTO, and Li3 battery) needed to be searched in advance. Note that though the costs of materials of batteries were similar, the labor cost and management cost widely vary, which causes large differences in the final costs and influences the key indices. For the viewpoint of this purely academic research, we only retrieved the data from research papers rather than focusing on specific market areas or specific time periods. However, to avoid the large difference of a specific index, three data-cancellation rules were set to judge and delete the extreme values: (1) the maximum value is more than or equal to two times the minimum values; (2) the difference of average values before and after deleting the maximum or minimum value is more than 10%; (3) from the normal distribution, the Z score (standard score) is higher than 1.23.

In Table 1, for supercapacitors, the averaged value of specific power was 7.3 (kW/kg) [24–26], the value of specific price [24] was 10,000 (USD/kWh), the averaged value of specific energy at constant volume was 0.0085 (kWh/L) [27], and the averaged value of specific energy at constant mass was 0.00484 (kWh/kg) [24,27,28]. The specific price and specific power was relatively high. Note that not all data-cancellation rules were satisfied (e.g., for specific power, the maximum value was two times the minimum value and the average values before and after deleting 10 were 7.3 and 5.95 (an 18.50% difference); however, the Z-score was 1.069, which was below 1.10, so all data were used for calculation).

Table 1. The performance indices of supercapacitors.

Parameter	Value	Average
Specific power (kW/kg)	5 [24]	7.3
	10 [25]	
	6.9 [26]	
Specific price (USD/kWh)	10,000 [24]	10,000
Power density (kWh/L)	0.0085 [27]	0.0085
Specific energy (kWh/kg)	0.005 [24]	0.00484
	0.0065 [27]	
	0.00302 [28]	

In Table 2, for LTO batteries, the average value of specific power was 2.763 (kW/kg) [2,17,29,30]; the value of specific price was 578.66 (USD/kWh) [2,29,31]; the average value of specific energy at constant volume was 0.138 (kWh/L) [30–32]; and the average value of specific energy at constant mass was 0.0635 (kWh/kg) [2,17,30–33]. Note that concerning the data-cancellation rules, for specific energy, the maximum value was nine times the minimum value, the average values before and after deleting 0.011 were 0.056 and 0.0635 (a 13.39% difference), and the Z-score was 1.62, which is higher than 1.10, so the data point 0.11 was deleted.

Table 2. The performance indices of LTO battery.

Parameter	Value	Average
Specific power (kW/kg)	3.2 [29]	2.7625
	2.25 [30]	
	2.4 [17]	
	3.2 [2]	
Specific price (USD/kWh)	432 [29]	578.66
	899 [2]	
	405 [31]	
Power density (kWh/L)	0.09 [30]	0.138
	0.147 [31]	
	0.177 [32]	
Specific energy (kWh/kg)	0.085 [33]	0.0635
	0.042 [30]	
	0.0715 [31]	
	0.046 [2]	
	0.0464 [17]	
	0.09 [32]	

In Table 3, for NCM (Li3) batteries, the average value of specific power was 0.416 (kW/kg) [2,17]; the value of specific price was 397.5 (USD/kWh) [2]; the averaged value of specific energy at constant volume was 0.400 (kWh/L) [31,32,34]; and the average value of specific energy at constant mass was 0.201 (kWh/kg) [2,17,30,31,34,35]. The values of specific energy at constant volume and specific energy at constant mass were relatively high. Note that concerning the data-cancellation rules, for specific power, the maximum value was 6.35 times the minimum value; the average values before and after deleting 2.3 were 0.887 and 0.416 (a 41.63% difference); and the Z-score was 1.49, which is higher than 1.10, so the data point 2.3 was deleted. From Tables 1–3, these performance indices were used for calculations.

4.2. GSA Results and Discussion

4.2.1. Optimization of Energy Sources

To fundamentally analyze four performance indices (mass, electric capacity, volume, and output power) with respect to size ratio and total price or electric capacity of the HEES, the GSA without the vehicle performance requirements (Equations (13)–(16)) was evaluated. There are two possible combinations: SC/Li3 and LTO/Li3 HEES. Figure 5 illustrates the performance of SC/Li3 with respect to total price and size ratio. In Figure 5a, at a fixed price, if the size ratio increases (more SC), the mass increases due to the high specific cost of the SC. In Figure 5b, at the fixed price, the electric capacity decreases as the SR increases due to the low energy density of the SC. In Figure 5c, at a fixed price, the volume increases

due to the low power density at the constant volume. In Figure 5d, at a constant price, the output power increases as the SR increases due to the high power density of the SC.

Table 3. The performance indices of the NCM (Li3) battery.

Parameter	Value	Average
Specific power (kW/kg)	0.433 [2]	0.416
	0.362 [2]	
	0.454 [17]	
Specific price (USD/kWh)	362 [2]	397.5
	433 [2]	
Power density (kWh/L)	0.37 [32]	0.400
	0.493 [31]	
	0.339 [34]	
Specific energy (kWh/kg)	0.174 [30]	0.201
	0.214 [31]	
	0.241 [17]	
	0.144 [2]	
	0.241 [2]	
	0.24 [35]	
	0.153 [34]	

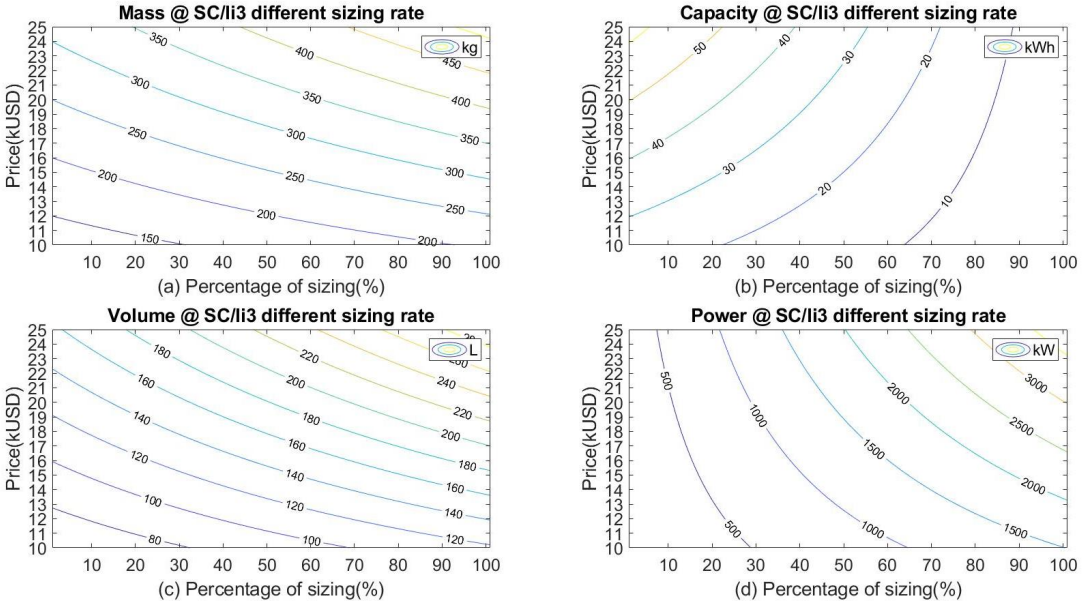


Figure 5. The performance indices of SC/Li3 HEES with respect to size ratio and total price: (**a**) mass, (**b**) stored energy, (**c**) volume, and (**d**) output power.

Another example is the LTO/Li3 HEES case. In Figure 6a, at a fixed price, if the size ratio increases (more LTO battery), the mass increases due to the lower specific energy at constant mass of the LTO battery referred to in Tables 2 and 3. In Figure 6b, at the fixed price, the electric capacity decreases as the SR increases due to the lower energy density of the LTO compared to Li3 batteries. In Figure 6c, at a fixed price, the occupied volume increases due to the lower specific energy at the constant volume. In Figure 6d, at a constant price, the output power increases as the SR increases because of the higher power density of the LTO batteries.

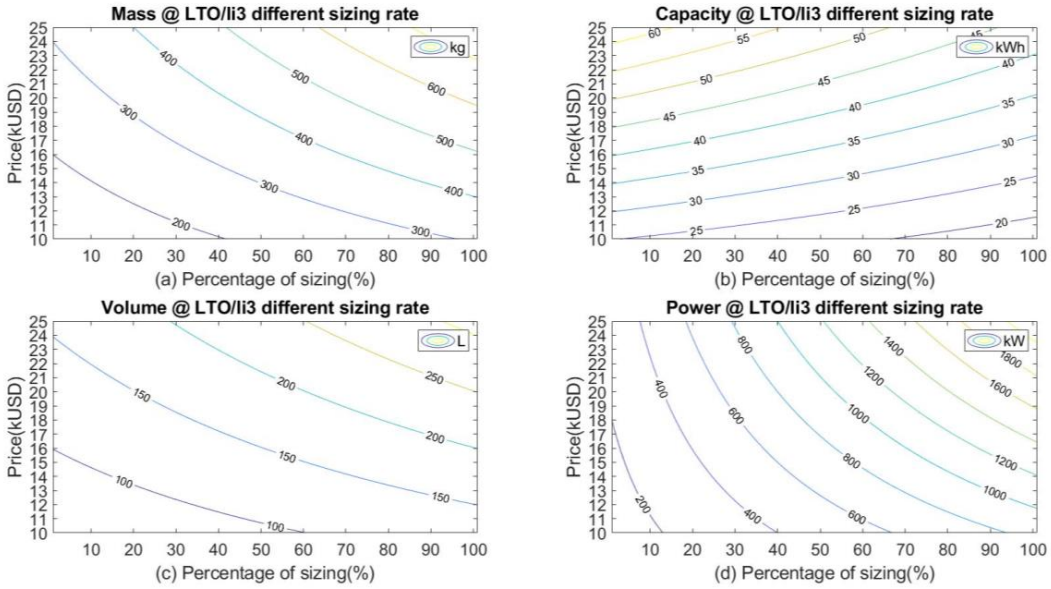


Figure 6. The performance indices of LTO/Li3 HEES with respect to size ratio and total price: (**a**) mass, (**b**) stored energy, (**c**) volume, and (**d**) output power.

From another view point, to investigate the relationship of multidimensional performance indices, we chose the electric capacity as the *y*-axis variable. In Figure 7a, at a fixed capacity, if the size ratio increases (more SC modules), the total cost increases due to the extremely high specific cost of the SC referred to in Tables 1 and 3. In Figure 7b, at the fixed capacity, the occupied volume of the HEES increases as the SR increases due to the lower energy density of the SC compared to Li3 batteries. To remain at the same capacity, the volume increases. In Figure 7c, at a fixed capacity, the HEES mass increases due to the lower specific energy at the constant volume of the SC. In Figure 7d, at a constant capacity, the output power increases as the SR increases due to the higher power density of the SC module.

For the case of the LTO/Li3 HEES, in Figure 8a, at a fixed electric capacity, if the size ratio increases (more LTO batteries), the total cost slightly increases due to the higher specific cost of the LTO compared with Li3 batteries, referred to in Tables 2 and 3. In Figure 8b, at the fixed capacity, the occupied volume of the HEES increases as the SR increases due to the lower energy density of the LTO compared to Li3 batteries. To remain at the same capacity, the volume increases. In Figure 8c, at a fixed capacity, the HEES mass increases due to the lower specific energy at the constant volume of the LTO battery. In Figure 8d, at a constant capacity, the output power increases as the SR increases due to the higher power density of the LTO module. From the example above, the relationship of performance indices with respect to the combinations of LTO/Li3 HEES and SC/Li3 HEES was constructed. It can be applied for the vehicle designs in Section 4.2.2.

4.2.2. Case Study of Five Types of EVs

In this Section, the GSA developed in Section 2.2 and the vehicle performance requirements and constraints in Section 3 were simulated.

Table 4 demonstrates the optimal sizing of the electric sedan. The vehicle performance requirements (constraints) were listed in Section 3.1. Table 4 shows that the case of LTO/Li3 combination was the best solution due to the lowest cost (33,111 USD) compared to that of the SC/Li3 case (33,842 USD). For the electric capacity, the optimal sizing was that the capacity of the LTO battery (as the high-power source) was 7.459 kWh, where the capacity of the Li3 battery (as the high-energy source) was 67.541 kWh. The size ratio was 9.9:90.1 where the total required capacity was 75 kWh. With the optimal sizing, the maximum output power of the LTO battery was 324.5 kW, while that of the Li3 battery was 139.8 kW.

The combined power exceeded the required power of 464 kW. The HEES mass (453 kg) was slightly higher than that of the SC/Li3 case (416 kg). Similarly, the occupied volume (222L) was slightly more than that of the SC/Li3 (212 L) case. The optimal position of the DC/DC converter was at the high-energy (Li3 battery) side. To prove that the GSA searched the optimal results in the electric sedan case, we manually and randomly selected cases that satisfied the physical constrains. For LTO/Li3 optimization, as the electric capacity was 7.55 and 67.45 kWh, respectively, the total price was calculated to be 33,151 USD. It increased by 0.12% compared to the GSA optimal result. The case with the highest price that satisfied the physical constraints was 33,181 USD, which was increased by 0.21%. In the case of SC/Li3 hybridization, the electric capacity was 0.33 and 74.64 kWh, respectively, where the price increased to 35,968 USD, which was increased by 6.3%. The case with the highest price that satisfied the physical constraints was 38,206 USD, which was increased by 12.89%.

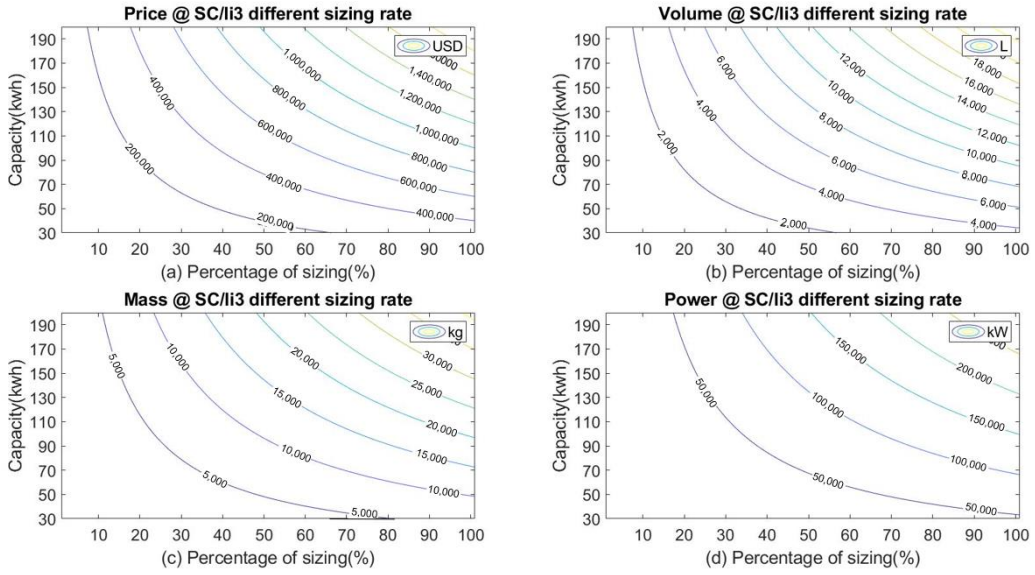


Figure 7. The performance indices of SC/Li3 HEES with respect to size ratio and electric capacity: (**a**) total cost, (**b**) volume, (**c**) mass and (**d**) output power.

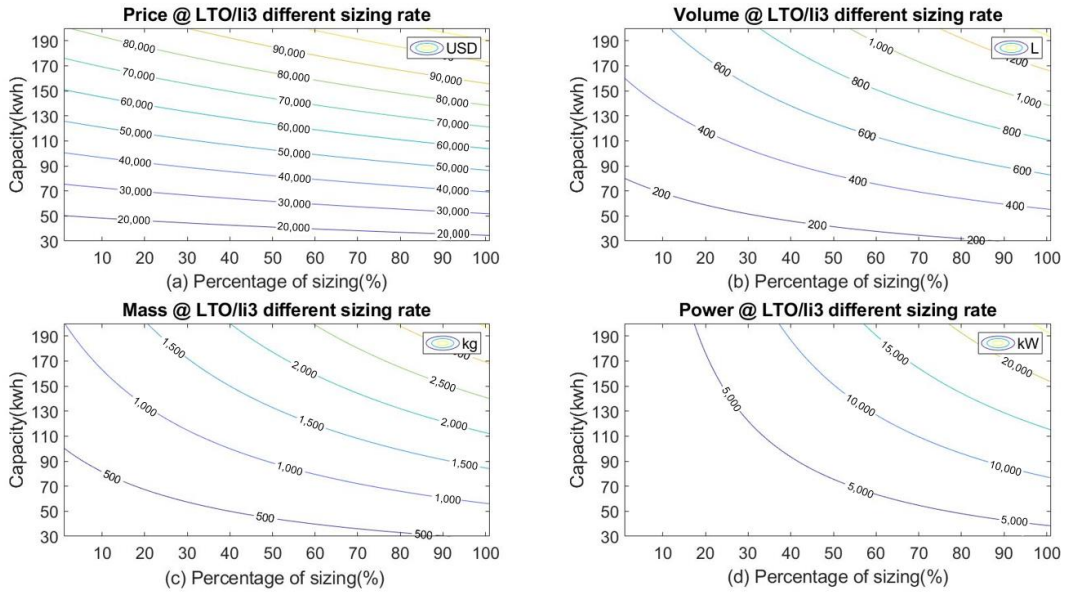


Figure 8. The performance indices of the LTO/Li3 HEES with respect to size ratio and electric capacity: (**a**) total cost, (**b**) volume, (**c**) mass, and (**d**) output power.

Table 5 demonstrates the optimal sizing of the electric forklift [36]. The case of SC/Li3 combination was the best solution, as the case of LTO/Li3 was unable to satisfy the required maximum output power. The HEES cost was calculated to be 24,973 USD. For the electric capacity, the optimal sizing was that the capacity of the SC module (as the high-power source) was 1.357 kWh, where the capacity of the Li3 battery (as the high-energy source) was 28.643 kWh. The size ratio was 4.52:95.48, where the total required capacity was 30 kWh. With the optimal sizing, the maximum output power of the SC was 2046 kW, while that of the Li3 battery was 59.3 kW. The combined power exceeded the required power of 2000 kW. The HEES mass was 422 kg, while the occupied volume was 231 L. The position of the DC/DC converter was at the SC side. To prove that the GSA was useful in the electric forklift case, we manually selected cases that satisfied the physical constrains. For SC/Li3 hybridization, as the electric capacity was 1.5 and 28.5 kWh, respectively, the total price was 26,347 USD. It increased 5.5% compared to the GSA optimal result. In the case that the electric capacity was 2 (SC) and 28 (Li3) kWh, respectively, the price was 31,154 USD, which was increased by 24.75%.

Table 6 demonstrates the optimal sizing of the long-distance electric bus. No matter LTO/Li3 or SC/Li3 cases, only using the Li3 battery was the best solution because of the long travelling distance. In this case, the Li3 battery cost was calculated to be 39,750 USD. For the electric capacity, the optimal sizing was that the capacity of the battery was 100 kWh. The HP:HE size ratio was 0:100, where the total required capacity was 100 kWh. The maximum output power of the battery was 442 kW. This power exceeded the required power of 300 kW. The HEES mass was 9212 kg, while the occupied volume was 200 L. There was no DC/DC converter for the HEES structure.

Table 7 demonstrates the optimal sizing of the short-distance electric bus. The case of LTO/Li3 combination was the best solution, as the case of SC/Li3 was unable to satisfy the required electric capacity described in Section 3. The HEES cost was calculated to be 34,914 USD. For the electric capacity, the optimal sizing was that the capacity of the LTO module (as the high-power source) was 32 kWh, where the capacity of the Li3 battery (as the high-energy source) was 40 kWh. The size ratio was 44.4:55.6, where the total required capacity was 72 kWh. With the optimal sizing, the maximum output power of the LTO battery was 1392 kW, while that of the Li3 battery was 83 kW. The combined power exceeded the required power of 528 kW. The HEES mass was 13,702 kg, while the occupied volume was 331 L. The position of DC/DC converter was at the Li3 battery side. To prove that the GSA searched the optimal results in the short-distance electric bus case, we selected cases in which the size ratio of LTO:Li3 was 50:50 (both were 36 kWh) and the total price was 35,589 USD. It increased 1.93% compared to the GSA optimal result. The case with the highest price that satisfied the physical constraints was 36,264 USD, which was increased by 3.86%, where the electric capacities were 40 and 32 kWh, respectively.

Table 8 demonstrates the optimal sizing of the electric sports car. The case of SC/Li3 combination was the best solution, as the case of LTO/Li3 was unable to satisfy the required maximum output power defined in Section 3. The HEES cost was calculated to be 45,315 USD. For the electric capacity, the optimal sizing was that the capacity of the SC module (as the high-power source) was 0.578 kWh, where the capacity of the Li3 battery (as the high-energy source) was 99.422 kWh. The size ratio was 0.58:99.42, where the total required capacity was 100 kWh. With the optimal sizing, the maximum output power of the SC was 871 kW, while that of the Li3 battery was 422 kW. The combined power exceeded the required power of 693 kW. The HEES mass was 595 kg, while the occupied volume was 298 L. The position of DC/DC converter was at the Li3 battery side.

Our simulation results showed that the designed GSA of the HEES will effectively search the optimal sizing and proper position of the DC/DC converter for various types of EVs.

Table 4. The GSA results for the case of electric sedan.

HEES Configuration	HP Capacity (kWh)	HE Capacity (kWh)	Total Capacity (kWh)	HP Power (kW)	HE Power (kW)	Power Demand (kW)	Weight (kg)	Volume (L)	Price (USD)	DCDC Position
LTO+Li3	7.459 (9.94%)	67.541 (90.05%)	75	324.50	139.78	464.25	453.49	222.62	33,111	HE
SC+Li3	0.216 (0.29%)	74.784 (99.71%)	75	345.79	154.78	455.64	416.69	212.06	33,842	HE

Table 5. The GSA results for the case of electric forklift.

HEES Configuration	HP Capacity (kWh)	HE Capacity (kWh)	Total Capacity (kWh)	HP Power (kW)	HE Power (kW)	Power Demand (kW)	Weight (kg)	Volume (L)	Price (USD)	DCDC Position
LTO+Li3	–	–	–	–	–	–	–	–	–	–
SC+Li3	1.357 (4.52%)	28.643 (95.48%)	30	2046.71	59.281	2000	422.87	231.14	24,973	HP

Table 6. The GSA results for the case of long-distance electric bus.

HEES Configuration	HP Capacity (kWh)	HE Capacity (kWh)	Total Capacity (kWh)	HP Power (kW)	HE Power (kW)	Power Demand (kW)	Weight (kg)	Volume (L)	Price (USD)	DCDC Position
LTO+Li3	0	100	100	0	441.62	300	9211.5	199.67	39,750	–
SC+Li3	0	100	100	0	441.62	300	9211.5	199.67	39,750	–

Table 7. The GSA results for the case of short-distance electric bus.

HEES Configuration	HP Capacity (kWh)	HE Capacity (kWh)	Total Capacity (kWh)	HP Power (kW)	HE Power (kW)	Power Demand (kW)	Weight (kg)	Volume (L)	Price (USD)	DCDC Position
LTO+Li3	32 (44.4%)	40 (55.6%)	72	1392.12	82.79	528.66	13,702	331.72	34,914	HE
SC+Li3	–	–	–	–	–	–	–	–	–	–

Table 8. The GSA results for the case of electric sports car.

HEES Configuration	HP Capacity (kWh)	HE Capacity (kWh)	Total Capacity (kWh)	HP Power (kW)	HE Power (kW)	Power Demand (kW)	Weight (kg)	Volume (L)	Price (USD)	DCDC Position
LTO+Li3	–	–	–	–	–	–	–	–	–	–
SC+Li3	0.578 (0.578%)	99.422 (99.422%)	100	871.77	422.26	692.67	595.1	298.4	45,315	HE

5. Conclusions

The conclusions of this study are summarized as follows:

(1) Performance indices and vehicle requirement: the average specific price, specific energy at a constant volume, specific energy at a constant mass, and specific power at a constant mass for three energy sources, SCs, LTO batteries, and Li3 batteries, were studied. The vehicle requirements including the maximum output power, vehicle acceleration, climbability, and maximum speed as the design constraints were formulated.

(2) The GSA of the HEES: the global search method with four steps including parameter input, definition of cost function and constraints, global search, and optimal results was developed.

(3) Numerical analysis of five types of EVs: by (1) and (2), five types of EVs including the electric sedan, electric forklift, long-distance electric bus, short-distance electric bus, and electric sports car were analyzed for optimal sizing of the HEES and the optimal position of the DC/DC converter with the lowest cost function. For the electric sedan, the optimal sizing was LTO+Li3 with a ratio of 9.9:90.1 and the DC/DC position was at Li3 side; for the electric forklift, the optimal sizing was SC+Li3 with a ratio of 4.5:95.5 and the DC/DC position was at SC side; for the long-distance electric bus, the optimal sizing was pure Li3 with no DC/DC converter; for the short-distance electric bus, the optimal sizing was LTO+Li3 with a ratio of 44.4:55.6 and the DC/DC position was at Li3 side; and for the electric sports car, the optimal sizing was SC+Li3 with a ratio of 0.58:99.42 and the DC/DC position was at Li3 side.

Utilizing these results, the integrated system and control designs of the HEES using the GSA, more applications for green energy sources, and different types of EVs will be studied in the future.

Author Contributions: Conceptualization and methodology, S.-Y.C., Y.-H.H., K.-K.J., G.-H.Y., and P.-L.S.; data search, C.-Y.C., Y.-H.H., C.-Y.C., and P.-L.S.; theories and equation derivation, S.-Y.C., Y.-H.H., and C.-Y.C.; software design and simulation, Y.-H.H. and C.-Y.C.; writing, Y.-H.H. and C.-Y.C. All authors have read and agreed to the published version of the manuscript.

Funding: This research was funded by Ministry of Science and Technology, grant number: MOST 110-2221-E-003-010-MY3, MOST 108-2628-E-003-001-MY3, MOST 110-2223-E-003-001-MY3 and MOST 111-2622-8-005-003-TE1; also was founded by National Chung-Shan Institute of Science and Technology, grant number: NCSIST-013-301(110).

Institutional Review Board Statement: Not applicable.

Informed Consent Statement: Not applicable.

Conflicts of Interest: The authors declare no conflict of interest.

References

1. Mourad, C.; Ibrahim, B.S.; Guillaume, K.; Rafik, N.; Claude, M. PMSM cogging torque reduction: Comparison between different shapes of magnet. In Proceedings of the 2012 First International Conference on Renewable Energies and Vehicular Technology (REVET), Nabeul, Tunisia, 26–28 March 2012; pp. 206–211.
2. Jan, B.; Thomas, N.; Raphaei, W.; Dirk, U.S. Dimensioning and Optimization of Hybrid Li-Ion Battery Systems for Evs. *World Electr. Veh. J.* **2018**, *9*, 1–18.
3. Naoki, N.; Feixiang, W.; Jung, T.L.; Gleb, Y. Li-ion battery materials: Present and future. *Materialstoday* **2015**, *18*, 252–264.
4. Un-Noor, F.; Padmanaban, S.; Mihet-Popa, L.; Mollah, M.N.; Hossain, E. A Comprehensive Study of Key Electric Vehicle (EV) Components, Technologies, Challenges, Impacts, and Future Direction of Development. *Energies* **2017**, *10*, 1217. [CrossRef]
5. Neigel, M.; Daniel, H.; Frédéric, G.; Loïc, B.; Kodjo, A. On the sizing and energy management of an hybrid multistack fuel cell—Battery system for automotive applications. *Int. J. Hydrogen Energy* **2017**, *42*, 1518–1526.
6. Wenlong, J.; Chean, H.L.; Shung, H.W.W.; Mou, L.D.W. Battery-supercapacitor hybrid energy storage system in standalone DC microgrids: A review. *IET Renew. Power Gener.* **2017**, *11*, 461–469.
7. Hanane, H.; Jamel, G.; Ahmed, C. Combination of Markov chain and optimal control solved by Pontryagin's Minimum Principle for a fuel cell/supercapacitor vehicle. *Energy Convers. Manag.* **2015**, *91*, 387–393.

8. Hassan, F. Fuel cell hybrid electric vehicle (FCHEV): Novel fuel cell/SC hybrid power generation system. *Energy Convers. Manag.* **2018**, *156*, 192–201.
9. Yujie, W.; Mince, L.; Zonghai, C. Experimental study of fractional-order models for lithium-ion battery and ultra-capacitor: Modeling, system identification, and validation. *Appl. Energy* **2020**, *278*, 115736.
10. Ibrahim, B.S.; Besma, B.; Demba, D. EV Energy Management Strategy Based on A Single Converter fed by a Hybrid Battery/Supercapacitor Power Source. In Proceedings of the 2014 First International Conference on Green Energy (ICGE), Sfax, Tunisia, 25–27 March 2014; pp. 246–250.
11. Saman, A.; Bathaee, S.M.T.; Amir, H.H. Improving fuel economy and performance of a fuel-cell hybrid electric vehicle (fuel-cell, battery, and ultra-capacitor) using optimized energy management strategy. *Energy Convers. Manag.* **2018**, *160*, 74–84.
12. Qiao, Z.; Weiwen, D.; Sumin, Z.; Jian, W. A Rule Based Energy Management System of Experimental Battery/Supercapacitor Hybrid Energy Storage System for Electric Vehicles. *J. Control Sci. Eng.* **2016**, *2016*, 1–17.
13. Yujie, W.; Zhendong, S.; Zonghai, C. Development of energy management system based on a rule-based power distribution strategy for hybrid power sources. *Energy* **2019**, *175*, 1055–1066.
14. Sisakat, S.T.; Barakati, S.M. Fuzzy Energy Management in Electrical Vehicles with Different Hybrid Energy Storage Topologies. In Proceedings of the 2015 4th Iranian Joint Congress on Fuzzy and Intelligent Systems (CFIS), Zahedan, Iran, 9–11 September 2015; pp. 1–6.
15. Chang, L.; Yujie, W.; Li, W.; Zonghai, C. Load-adaptive real-time energy management strategy for battery/ultracapacitor hybrid energy storage system using dynamic programming optimization. *J. Power Sources* **2019**, *438*, 227024.
16. Farouk, O.; Jürgen, R.; Angelika, H. Power Management Optimization of a Fuel Cell/Battery/Supercapacitor Hybrid System for Transit Bus Applications. *IEEE Trans. Veh. Technol.* **2016**, *65*, 5783–5788.
17. Raphael, W.; Volker, D.; Jan, B.; Dirk, U.S. Optimized operation of hybrid battery systems for electric vehicles using deterministic and stochastic dynamic programming. *J. Energy Storage* **2017**, *14*, 22–38.
18. Ding, N.; Prasad, K.; Lie, T.T. Design of a hybrid energy management system using designed rule-based control strategy and genetic algorithm for the series-parallel plug-in hybrid electric vehicle. *Int. J. Energy Res.* **2021**, *45*, 1627–1644. [CrossRef]
19. Hou, Z.; Guo, J.; Xing, J.; Guo, C.; Zhang, Y. Machine learning and whale optimization algorithm based design of energy management strategy for plug-in hybrid electric vehicle. *IET Intell. Transp. Syst.* **2021**, *15*, 1076–1091. [CrossRef]
20. Krishna, V.S.; Hari, O.B.; Dheerendra, S. Development of an adaptive neuro-fuzzy inference system–based equivalent consumption minimisation strategy to improve fuel economy in hybrid electric vehicles. *IET Electr. Syst. Transp.* **2021**, *11*, 171–185.
21. Raphael, W.; Volker, D.; Dirk, U.S. Assessing the potential of an electric vehicle hybrid battery system comprising solid-state lithium metal polymer high energy and lithium-ion high power batteries. *J. Energy Storage* **2018**, *18*, 175–184.
22. Raphael, W.; Volker, D.; Dirk, U.S. Assessing the potential of a hybrid battery system to reduce battery aging in an electric vehicle by studying the cycle life of a graphite|NCA high energy and a LTO|metal oxide high power battery cell considering realistic test profiles. *Appl. Energy* **2018**, *226*, 197–212.
23. Raphael, W.; Volker, D.; Dirk, U.S. Energy Optimal operation of Hybrid Battery Systems and Comparison to a Single-Cell Reference System for Electric Vehicles Including the Aged State of High Energy Cells. *World Electr. Veh. J.* **2016**, *8*, 315–325.
24. Balali, Y.; Stegen, S. Review of energy storage systems for vehicles based on technology, environmental impacts, and costs. *Renew. Sustain. Energy Rev.* **2021**, *135*, 110185. [CrossRef]
25. Kasimalla, V.K.; Velisala, V. A review on energy allocation of fuel cell/battery/ultracapacitor for hybrid electric vehicles. *Int. J. Energy Res.* **2017**, *42*, 4263–4283. [CrossRef]
26. Wieczorek, M.; Lewandowski, M. A mathematical representation of an energy management strategy for hybrid energy storage system in electric vehicle and real time optimization using a genetic algorithm. *Appl. Energy* **2014**, *192*, 222–233. [CrossRef]
27. Ahmed, A.; Sheikh, M.H.R.; Atia, T.A.; Juliana, Z.; Md, A.I.; Abul, K.A. Advanced materials and technologies for hybrid supercapacitors for energy storage—A review. *J. Energy Storage* **2019**, *25*, 100852.
28. Kavil, J.; Anjana, P.M.; Roshni, C.P.; Periyat, P.; Raj, K.G.; Rakhi, R.B. Multifunctional nanohybrid material from discarded razor blades as cost-effective supercapacitor electrodes and oil-spill cleaners. *Appl. Surf. Sci.* **2019**, *487*, 109–115. [CrossRef]
29. Weichao, Z.; Jianwei, Y.; Ziyou, S.; Guodong, Y.; Guangmin, L. Comparison of semi-active hybrid battery system configurations for electric taxis application. *Appl. Energy* **2020**, *259*, 114171.
30. Nikolian, A.; Jaguemont, J.; de Hoog, J.; Goutam, S.; Omar, N.; Van, D.B.P.; Van, M.J. Complete cell-level lithium-ion electrical ECM model for different chemistries (NMC, LFP, LTO) and temperatures (−5 °C to 45 °C)–Optimized modelling techniques. *Int. J. Electr. Power Energy Syst.* **2018**, *98*, 133–146. [CrossRef]
31. Thomas, N.; Philipp, S.; Matthias, K.; Dirk, U.S. Lithium titanate oxide battery cells for high-power automotive applications–Electro-thermal properties, aging behavior and cost considerations. *J. Energy Storage* **2020**, *31*, 101656.
32. Toshiba International Corporation, Super Charge Ion Battery. 20 Amp Hour Cell Datasheet. Available online: http://www.toshiba.com/tic/ (accessed on 9 August 2021).
33. Xiaobin, Z.; Huei, P.; Hewu, W.; Minggao, O. Hybrid Lithium Iron Phosphate Battery and Lithium Titanate Battery Systems for Electric Buses. *IEEE Trans. Veh. Technol.* **2018**, *67*, 956–965.
34. Delta Electronics, Inc., Lithium-ion Battery High Capacity. Delta P140-222-5 Datasheet. Available online: https://www.deltaww.com/en-US/index (accessed on 9 August 2021).

35. Benveniste, G.; Rallo, H.; Casals, L.C.; Merino, A.; Amante, B. Comparison of the state of Lithium-Sulphur and lithium-ion batteries applied to electromobility. *J. Environ. Manag.* **2018**, *226*, 1–12. [CrossRef] [PubMed]
36. Théophile, P.; Tedjani, M.; Sylvain, D.; Damien, F.; Wilfried, U. Sizing of Lithium-Ion Battery/Supercapacitor Hybrid Energy Storage System for Forklift Vehicle. *Energies* **2020**, *18*, 4518.